NEUROSCIENCE

Hypothalamic circuitry underlying stress-induced insomnia and peripheral immunosuppression

Shi-Bin Li[1,2]*, Jeremy C. Borniger[1,2†], Hiroshi Yamaguchi[1,2‡], Julien Hédou[3], Brice Gaudilliere[3], Luis de Lecea[1,2]*

The neural substrates of insomnia/hyperarousal induced by stress remain unknown. Here, we show that restraint stress leads to hyperarousal associated with strong activation of corticotropin-releasing hormone neurons in the paraventricular nucleus of hypothalamus (CRH^{PVN}) and hypocretin neurons in the lateral hypothalamus ($Hcrt^{LH}$). CRH^{PVN} neurons directly innervate $Hcrt^{LH}$ neurons, and optogenetic stimulation of LH-projecting CRH^{PVN} neurons elicits hyperarousal. CRISPR-Cas9–mediated knockdown of the *crh* gene in CRH^{PVN} neurons abolishes hyperarousal induced by stimulating LH-projecting CRH^{PVN} neurons. Genetic ablation of Hcrt neurons or *crh* gene knockdown significantly counteracts restraint stress–induced hyperarousal. Single-cell mass cytometry by time of flight (CyTOF) revealed extensive changes to immune cell distribution and functional responses in peripheral blood during hyperarousal upon optogenetic stimulation of CRH^{PVN} neurons simulating stress-induced insomnia. Our findings suggest both central and peripheral systems are synergistically engaged in the response to stress via CRH^{PVN} circuitry.

INTRODUCTION

A brief exposure to a stressor imposes a persistent imprint on the brain (*1*). Insomnia is among the most prevalent stress-related complaints, and clarification of the mechanism underlying stress-induced insomnia is essential for developing effective treatment. Accumulated evidence has shown that wakefulness-promoting brain regions are involved in the neural response to stress (*2*). In addition, changes in adaptive and maladaptive immune responses have been empirically linked to stress exposure (*3*). However, the explicit neural circuitry integrating behavioral (e.g., insomnia) and physiological (e.g., immunosuppression) effects of stress remains unclear.

Stress induces insomnia/hyperarousal in humans (*4*) and rodent model (*2*). Transitions from sleep to wakefulness can be elicited upon optogenetic activation of the hypocretin/orexin (Hcrt) system (*5*), noradrenergic locus coeruleus (*6*), dopaminergic neurons in ventral tegmental area (VTA) (*7*) and dorsal raphe (*8*), and/or the cholinergic basal forebrain, among others (*9*, *10*). Despite the strong evidence demonstrating a causal relationship between neuronal ensembles and behavioral wakefulness, whether these same neuronal populations are recruited during stress exposure remains unknown. Some arousal-promoting brain nuclei are preferably active during appetitive sensory inputs. For example, fiber photometry recording from dopaminergic neurons in the VTA (*7*) and dorsal raphe nucleus (*8*) in male mice showed maximum activity during presence of palatable food and female mice, suggesting their association with positive valence. Furthermore, the observation that reward buffers the CRH^{PVN} neuronal activities following footshock stressor (*11*) suggests that the reward-related neuronal ensembles are unlikely implicated in stress circuitry. Both positive and negative stimuli are able to elicit Hcrt neuronal activities (*12*). These studies indicate different arousal-promoting brain nuclei may mediate arousal in response to various stimuli depending on their respective valence (either positive or negative). A well-defined neural circuitry linking stress to arousal has yet to be adequately described.

Psychosocial stress has well-known effects on systemic immune responses (*3*). Specifically, chronic stressors suppress both cellular and humoral measures (*13*). For example, in a classic study of chronically stressed caregivers of patients with dementia, Kiecolt-Glaser *et al.* observed marked decrements in three separate measures of cellular immunity (*14*). In animal models, psychological stress (e.g., via restraint stress) causes thymic involution (along with T cell apoptosis) and suppresses granulocyte and macrophage migration to the location of inflammatory challenge, putatively via a glucocorticoid-dependent mechanism (*15*). A major driver of immune responses to stressors are glucocorticoids secreted from the adrenal cortex, downstream of the hypothalamic-pituitary-adrenal (HPA) axis (*16*). CRH^{PVN} neurons serve as the initial node in this axis, transducing the neuronal signal of stress into an endocrine output (i.e., glucocorticoid secretion). The actions of the HPA axis are fundamentally coupled to arousal, as sleep disruption powerfully drives HPA activation and glucocorticoid secretion in human (*17*). Despite the clear effects of stress and stress-induced arousal on the immune system, an understanding of the neural circuitry underlying this phenomenon is lacking.

We hypothesized that insomnia/hyperarousal and peripheral immunosuppression may share the same neural substrates under stress. We performed a series of experiments with transgenic mice to test this hypothesis. After identifying that both stress-associated CRH^{PVN} neurons and arousal-promoting $Hcrt^{LH}$ neurons are activated by restraint stress, we demonstrated that $Hcrt^{LH}$ neurons are monosynaptically innervated by CRH^{PVN} neurons. We then observed that the activity of CRH^{PVN} neurons is not required for natural sleep-to-wake transitions but associates with stress exposure. Mild optogenetic stimulation of CRH^{PVN}, but not $Hcrt^{LH}$ neurons, elicited persistent wakefulness mimicking insomnia induced by restraint stress. Genetic ablation of Hcrt neurons or knockdown of *crh* gene in CRH^{PVN} neurons counteracted insomnia/hyperarousal induced by optogenetic

[1]Department of Psychiatry and Behavioral Sciences, Stanford University School of Medicine, 1201 Welch Road, Stanford, CA 94305, USA. [2]Wu Tsai Neurosciences Institute, Stanford University, Stanford, CA 94305, USA. [3]Department of Perioperative and Pain Medicine, Stanford University School of Medicine, Stanford, CA 94305, USA.
*Corresponding author. Email: lishibin@stanford.edu (S.-B.L.), llecea@stanford.edu (L.d.L.)
†Present address: Cold Spring Harbor Laboratory, One Bungtown Road, Cold Spring Harbor, NY 11724, USA
‡Present address: Department of Neuroscience II, Research Institute of Environmental Medicine, Nagoya University, Nagoya 464-8601, Japan

stimulation or restraint stress. Unbiased mass cytometry by time of flight (CyTOF) analysis revealed optogenetic stimulation of CRH^{PVN} neurons leads to peripheral immunosuppression simulating the physiological effect due to stress. These data suggest that connections between CRH^{PVN} and $Hcrt^{LH}$ neurons drive stress-induced insomnia, partially at least, and that activation of CRH^{PVN} neurons is sufficient to elicit stress-induced immunosuppression.

RESULTS

Restraint stress causes strong cFos expression in CRH^{PVN} and $Hcrt^{LH}$ neurons

To reveal the specific neuronal responses to stress exposure, we investigated the stress-related paraventricular nucleus of the hypothalamus (PVN) and the arousal-related brain region the lateral hypothalamus (LH). We subjected mice to restraint stress, a well-established robust and noninvasive stress paradigm (*18*) and performed cFos antibody staining at different time points following restraint stress. We found a large number of cells around the PVN and LH to be cFos positive (fig. S1), consistent with earlier work showing cFos activity upon exposure to cage exchange stress in rats (*2*). Antibody staining in the same slices revealed that the vast majority of PVN cFos-positive neurons coexpress corticotropin-releasing hormone (CRH; also known as corticotropin-releasing factor), and a major population of LH cFos-positive neurons are hypocretinergic (fig. S1), a group of neurons that play a major role in promoting and stabilizing wakefulness (*5*).

CRH^{PVN} neurons directly innervate $Hcrt^{LH}$ neurons

The PVN consists of a constellation of several neuronal types including those that secrete the neuropeptides CRH, arginine vasopressin (AVP), and oxytocin (OXT) (*19*). It was unclear which cell type in the PVN directly makes synapses onto $Hcrt^{LH}$ neurons, despite previous reports that the PVN is an upstream partner of Hcrt neurons (*12*, *20*). We used the EnvA-pseudotyped glycoprotein (G)–deleted rabies virus (EnvA + RV*d*G) system (*21*) to trace the monosynaptic inputs to Hcrt neurons and found a major population of PVN neurons directly projected to Hcrt neurons. We further performed antibody staining in the PVN and found around 60% of the RV*d*G-labeled PVN neurons were CRH positive and about half of the CRH^{PVN} neurons were labeled by the RV*d*G (Fig. 1, A to E). AVP and OXT neurons, another two major populations of neurons intermingled with CRH neurons in the PVN (*19*), were labeled with a much lower ratio (Fig. 1, F to J and K to O). We then injected AAV-Retro vectors (*22*) carrying enhanced yellow fluorescent protein (eYFP) to the LH of CRH::Cre, AVP::Cre, and OXT::Cre mouse lines, respectively, and observed that nearly 70% of CRH neurons projected to the LH containing Hcrt neurons (fig. S2, A to E). Notably, about 60% AVP neurons were labeled by AAV-Retro vectors (fig. S2, F to J), suggesting AVP^{PVN} neurons may target neuronal populations that are distinct from Hcrt neurons in the LH given the cell type–specific monosynaptic tracing of Hcrt neurons in Fig. 1. These two sets of experiments demonstrated CRH^{PVN} neurons are the primary population targeting $Hcrt^{LH}$ neurons, and established a direct link between neurons orchestrating stress and arousal. Both

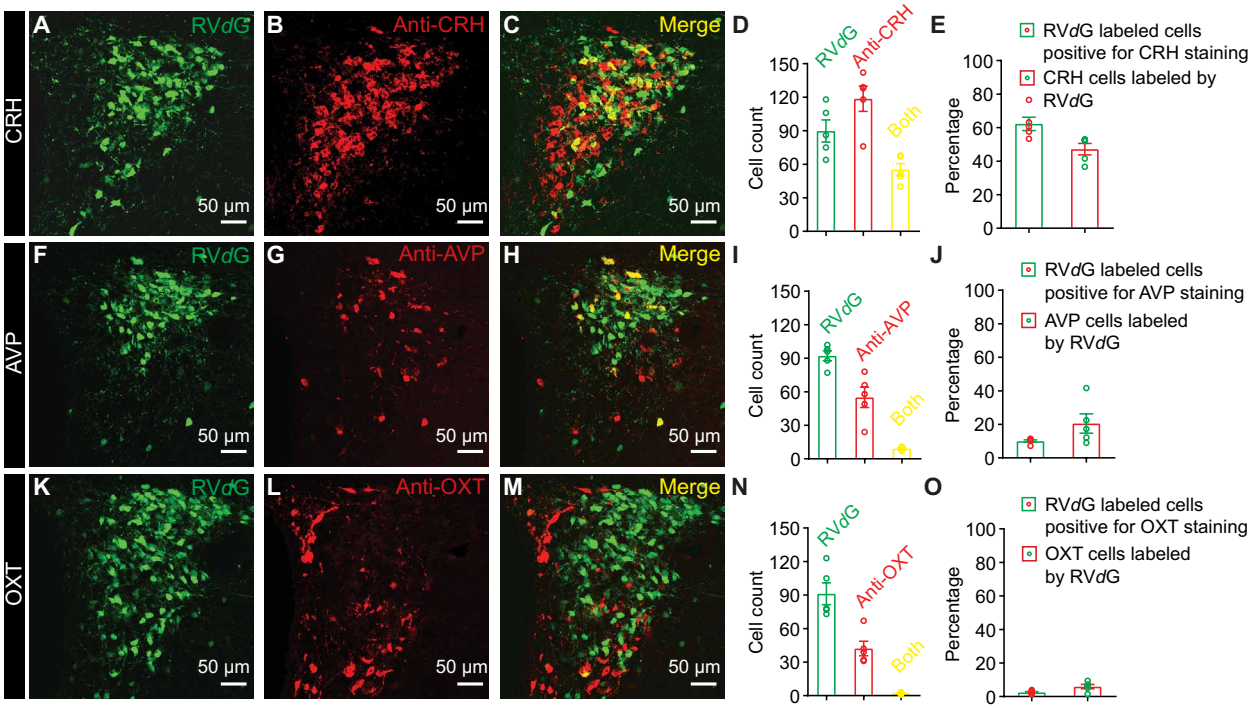

Fig. 1. CRH^{PVN} neurons directly innervate $Hcrt^{LH}$ neurons with monosynaptic contacts. (**A** to **E**) Representative slice containing PVN neurons labeled by RV*d*G (A), antibody staining against CRH (B), merged slice (C), cell counts of RV*d*G-labeled neurons, CRH-positive neurons and both-positive neurons (D), and percentages of RV*d*G-labeled neurons positive for CRH staining and CRH neurons labeled by RV*d*G (E). (**F** to **J**) Representative slice containing PVN neurons labeled by RV*d*G (F), antibody staining against AVP (G), merged slice (H), cell counts of RV*d*G-labeled neurons, AVP-positive neurons and both-positive neurons (I), and percentages of RV*d*G-labeled neurons positive for AVP staining and AVP neurons labeled by RV*d*G (J). (**K** to **O**) Representative slice containing PVN neurons labeled by RV*d*G (K), antibody staining against OXT (L), merged slice (M), cell counts of RV*d*G-labeled neurons, OXT-positive neurons and both-positive neurons (N), and percentages of RV*d*G-labeled neurons positive for OXT staining and OXT neurons labeled by RV*d*G (O) ($n = 5$ mice).

tracing strategies identified only limited OXT neurons projected to the LH (Fig. 1, K to O, and fig. S2, K to O), confirming earlier observations (*23*).

Activity of CRH^{PVN} neurons is not a prerequisite for natural sleep-to-wake transitions

We then monitored the activity of CRH^{PVN} neurons in CRH::Cre mice and Hcrt^{LH} neurons in Hcrt::Cre mice by measuring Ca^{2+} transients during natural sleep/wake transitions in their home cages using fiber photometry (Fig. 2). CRH^{PVN} neurons showed minimal changes in activity during natural sleep/wake transitions (Fig. 2, A to C). However, Hcrt^{LH} neurons were highly active during wakefulness (Fig. 2, D to F) independent of duration, confirming earlier findings (*24*, *25*). These experiments demonstrated that activation of Hcrt neurons does not require CRH^{PVN} neuronal activity during natural sleep-to-wake transitions.

Stress elicits strong CRH^{PVN} and Hcrt^{LH} neuronal activity

We further investigated how CRH^{PVN} and Hcrt^{LH} neurons change their activity in response to various salient stimuli involving novelty, social, appetitive, and aversive components. Generally, aversive stimuli such as 2,3,5-trimethyl-3-thiazoline (TMT; a component of fox odor), restraint stress, open arm of the elevated plus maze (EPM), and manual grabbing triggered substantial CRH^{PVN} neuronal activity, whereas neutral or appetitive stimuli including novelty (novel Falcon tube), female mice, high-fat diet (HFD) elicited CRH^{PVN} neuronal activity to a lesser extent (Fig. 3, A and B). The increase in CRH^{PVN} neuronal activity upon aversive stimuli is consistent with previous work using aversive stimuli including forced swim test, tail-restraint test, overhead object, TMT, looming disk (*26*), and white noise (*27*). Hcrt^{LH} neurons displayed strong neuronal activity to various stimuli regardless of stimulus valence (Fig. 3, C and D). Notably, restraint stress triggered robust activity in both of CRH^{PVN} and Hcrt^{LH} neurons especially at the beginning of restraint stress exposure (Fig. 3, "Restraint" panel). Synergistic activation of CRH^{PVN} and Hcrt^{LH} neurons during restraint stress is consistent with our observation of cFos staining as described in fig. S1.

Mild optogenetic stimulation of LH-projecting CRH^{PVN} neurons leads to insomnia

Because CRH^{PVN} neurons are sensitive to stressful stimuli, we hypothesized that the neuronal circuitry connecting CRH^{PVN} and Hcrt^{LH} neurons drives hyperarousal/insomnia in response to stress exposure. We thus conducted a series of optogenetic experiments in Hcrt::Cre (Fig. 4A), CRH::Cre (Fig. 4E), CRH::Cre-ATA3 mice (*28*), which have their Hcrt neurons ablated (Fig. 4I and fig. S3, E to H), and CRH::Cre-Cas9 mice with the *crh* gene disrupted using CRISPR-Cas9 technology (*29*) in CRH^{PVN} neurons (Fig. 4M and fig. S4). We used a mild optogenetic stimulation paradigm (i.e., 15-ms 473-nm blue light pulse at 0.1 Hz for 6 hours starting from the beginning of the light phase) with neglectable effects on Hcrt^{LH} neurons in changing the amount of sleep/wakefulness (Fig. 4, A to D and Q to S, and fig. S5, A and E). Notably, this same optogenetic stimulation of CRH^{PVN} neurons labeled with ChR2-eYFP by AAV-Retro vectors injected to LH significantly increased the amount of wakefulness (†$P < 0.0005$; Fig. 4, E to H and Q to S, and fig. S5, B and F), here defined as

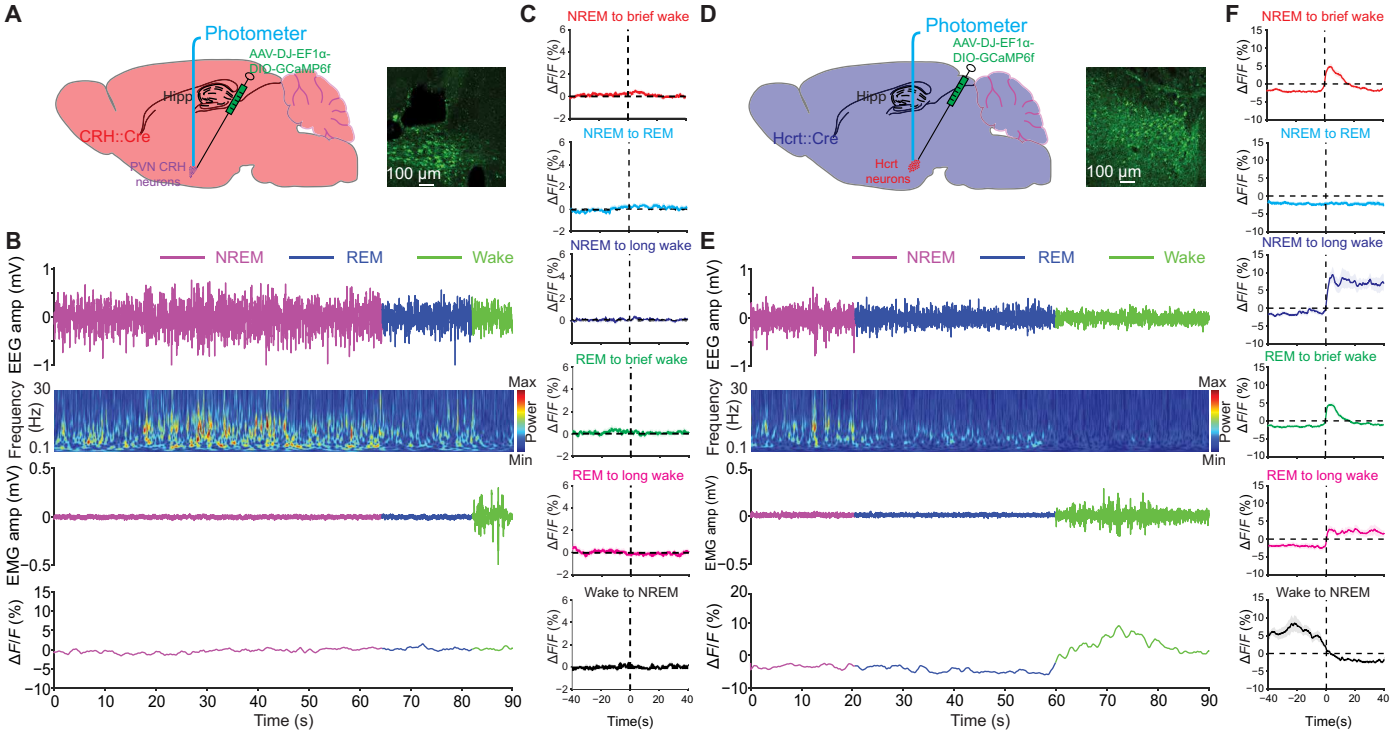

Fig. 2. CRH^{PVN} and Hcrt^{LH} neuronal activity during natural sleep/wake transitions. (**A**) Diagram of fiber photometry recording from CRH^{PVN} neurons. (**B**) Representative EEG, EEG power spectra, EMG, and CRH^{PVN} GCaMP trace recorded simultaneously during a 90-s natural sleep/wake transition episode from a CRH::Cre mouse. (**C**) No obvious fluctuations of Ca^{2+} transients in CRH^{PVN} neurons during natural sleep/wake transitions. (**D**) Diagram of fiber photometry recording from Hcrt^{LH} neurons. (**E**) Representative EEG, EEG power spectra, EMG, and Hcrt^{LH} GCaMP trace recorded simultaneously during a 90-s natural sleep/wake transition episode from a Hcrt::Cre mouse. (**F**) Strong Ca^{2+} transients correlate with wakefulness in Hcrt^{LH} neurons during natural sleep/wake transitions. $n = 7$ for (C), $n = 6$ for (F).

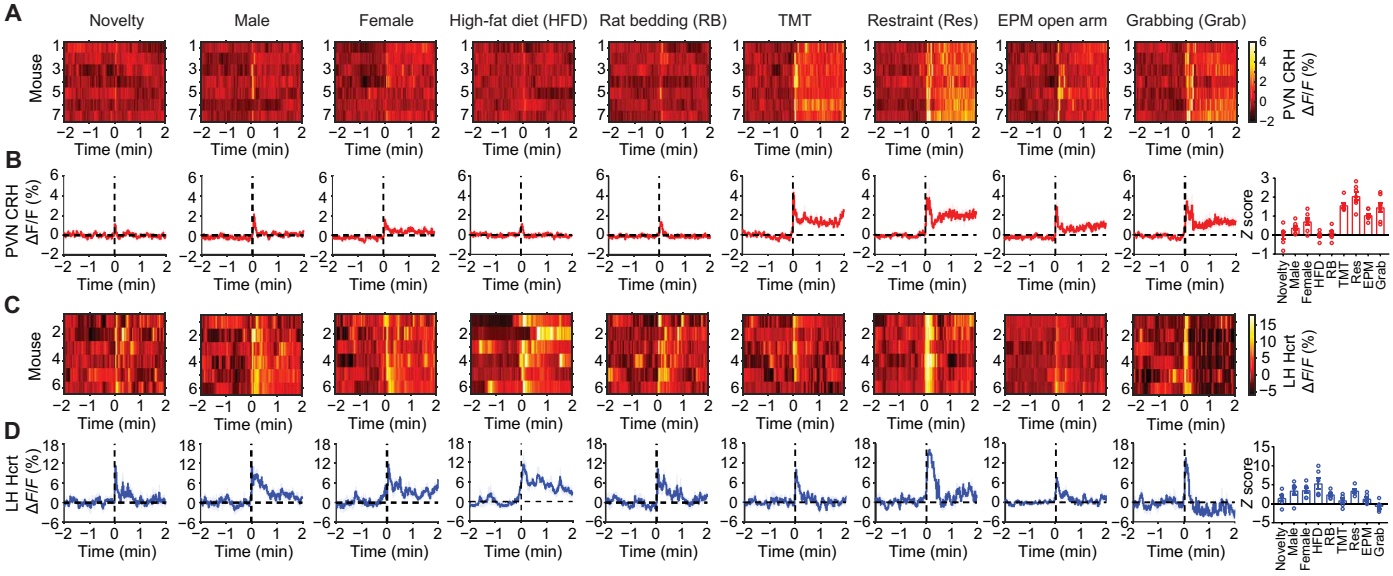

Fig. 3. CRH^{PVN} and Hcrt^{LH} neuronal activity during exposure to salient stimuli. (**A** and **B**) CRH^{PVN} neurons and (**C** and **D**) Hcrt^{LH} neurons respond to distinct stimuli. Note aversive stimuli including predator fox odor (TMT), restraint stress (Res), EPM open arm (mimicking anxiety condition), and manual grabbing (Grab) lead to strong CRH^{PVN} neuronal activities. Hcrt^{LH} neurons respond strongly to social, appetitive, and restraint stimuli (A and B, $n = 7$; C and D, $n = 6$).

insomnia/hyperarousal. This observation is consistent with earlier report that intracerebroventicular injection of CRH causes long-lasting wakefulness (*30*). Optogenetic stimulation of LH-projecting CRH^{PVN} neurons of the CRH::Cre-ATA3 mice without Hcrt neurons (fig. S3, E to H) also triggered a robust increase in wakefulness, but the effect was significantly smaller when compared with the condition with intact Hcrt neurons (†$P < 0.0005$; Fig. 4, I to L and Q to S, and fig. S5, C and G). We further investigated whether CRH release is necessary for the optogenetically induced arousal response. We generated viruses carrying single guide RNAs (sgRNAs) to selectively disrupt the *crh* gene in CRH^{PVN} neurons of CRH::Cre-Cas9 mice (fig. S4). Optogenetic stimulation of CRH^{PVN} neurons projecting to LH from *crh* gene–disrupted mice failed to increase wakefulness (Fig. 4, M to P and Q to S, and fig. S5, D and H), suggesting a critical role of CRH in activating downstream arousal-promoting brain nuclei including the Hcrt^{LH} neurons (*31*). Furthermore, we identified that CRH, AVP, and OXT neurons in the PVN are non-GABAergic as revealed by antibody staining in Vgat::Cre-tdTomato slices (fig. S6), supporting earlier studies demonstrating that CRH^{PVN} neurons are glutamatergic/excitatory (*32*, *33*).

Disruption of CRH^{PVN}-Hcrt^{LH} circuitry compromises restraint stress–induced insomnia/hyperarousal

Given the observation of robust wakefulness upon optogenetic activation of LH-projecting CRH^{PVN} neurons (Fig. 4 and fig. S5), we then evaluated whether the CRH^{PVN}-Hcrt^{LH} pathway is relevant to hyperarousal/insomnia under stress. We subjected three genotypes of mice to restraint stress with intact or disrupted CRH^{PVN}-Hcrt^{LH} neuronal circuitry. We monitored electroencephalography (EEG)/electromyography (EMG) with a 10-min restraint session (*18*) in CRH::Cre mice, CRH::Cre-ATA3 mice with a genetic ablation of Hcrt neurons, and CRH::Cre-Cas9 mice with the *crh* gene disrupted bilaterally in PVN. A 10-min restraint stress session significantly delayed the nonrapid eye movement (NREM) and rapid eye movement (REM) sleep onset (Fig. 5A). Either genetic ablation of Hcrt neurons or CRISPR-Cas9–mediated disruption of the *crh* gene in CRH^{PVN} neurons significantly reduced the latency to NREM sleep onset compared with the mice with intact Hcrt neurons and *crh* gene, suggesting that these neurons play a synergistic role in stress-induced insomnia/hyperarousal. However, this acute 10-min restraint stress did not introduce notable changes to the general sleep/wake architecture in these three genotypes (Fig. 5, B to J). We further compared the basic sleep/wake patterns among these three genotypes and found significantly higher amount of REM sleep in CRH::Cre-ATA3 mice with Hcrt neurons ablated, and in CRH::Cre-Cas9 mice with disrupted *crh* gene in CRH^{PVN} neurons by sgRNAs (fig. S7, A to F). Higher amount of REM sleep in ATA3 mice confirmed earlier observation in the same ATA3 mouse line (*34*). The higher amount of REM sleep in CRH::Cre-Cas9 mice with disrupted *crh* gene appeared to be previously unidentified to the best of our knowledge. In addition, a single acute 10-min restraint stress did not change the pattern of difference observed in nonrestraint condition (fig. S7, G to L).

Optogenetic activation of CRH^{PVN} neurons causes immunosuppression

As activation of stress circuitry drives changes in whole-body physiology (i.e., "fight or flight" response), we investigated the immunomodulatory effects of CRH^{PVN} neuron stimulation using single-cell mass CyTOF (*35*). We assessed changes in the distribution of circulating immune cells (Fig. 6) as well as alterations in intracellular signaling cascades (fig. S8) in response to a single session of CRH^{PVN} optogenetic stimulation. CRH neuron stimulation resulted in marked alterations in peripheral immune cell distribution (Fig. 6B). Specifically, we observed a reduction in the frequencies of natural killer (NK) cells, MHCII^{+} dendritic cells, inflammatory (Ly6C^{Hi}), patrolling (Ly6C^{low}) monocytes, B cells (total), T helper 1 (T_H1) TBet^{+} T cells, and CD4^{+} T cells (total) in response to optogenetic stimulation (Fig. 6, C and D). These findings indicate that CRH neuronal stimulation altered

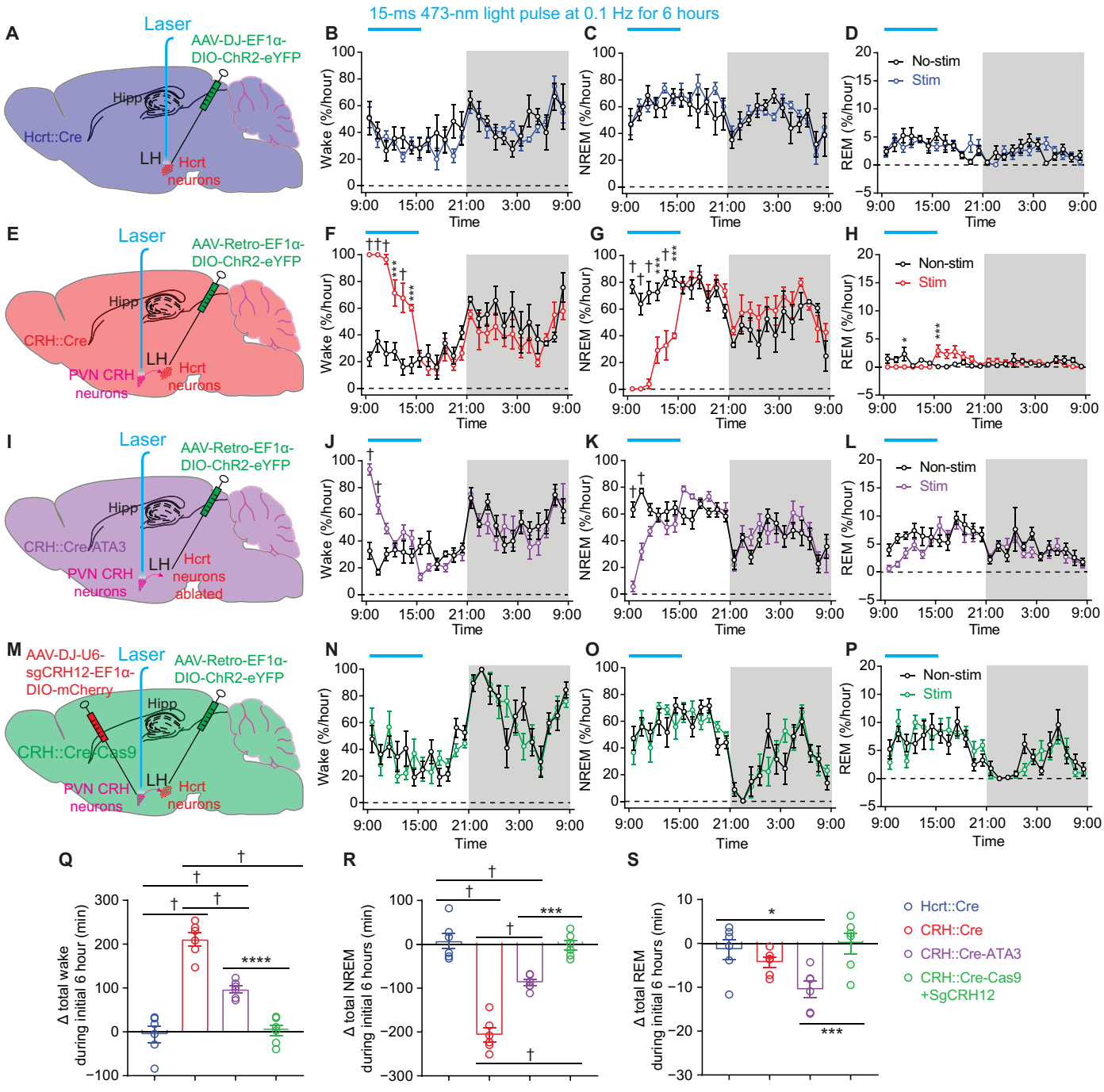

Fig. 4. Optogenetic stimulation of CRH^{PVN} neurons elicits insomnia-like behavior. (**A**) Diagram of viral injection and fiber placement for optogenetic stimulation of Hcrt neurons in Hcrt::Cre mice. (**B** to **D**) Prolonged mild optogenetic stimulation of Hcrt^{LH} neurons had no significant effect on sleep/wake pattern in Hcrt::Cre mice. (**E**) Diagram of viral injection and fiber placement for optogenetic stimulation of LH-projecting CRH^{PVN} neurons in CRH::Cre mice. (**F** to **H**) Prolonged mild optogenetic stimulation of CRH^{PVN} neurons elicited consolidated wakefulness in CRH::Cre mice. (**I**) Diagram of viral injection and fiber placement for optogenetic stimulation of CRH^{PVN} neurons projecting to LH in CRH::Cre-ATA3 mice without Hcrt neurons. (**J** to **L**) Prolonged mild optogenetic stimulation of CRH^{PVN} LH-projecting neurons significantly increased the amount of wakefulness in the absence of Hcrt neurons. (**M**) Diagram of viral injection and fiber placement for optogenetic stimulation of LH-projecting CRH^{PVN} neurons with *crh* gene disrupted. (**N** to **P**) Disruption of *crh* gene in CRH^{PVN} neurons compromised the strong wakefulness-promoting effect elicited by stimulating LH-projecting CRH^{PVN} neurons in CRH::Cre-Cas9 mice. (**Q** to **S**) Prolonged mild optogenetic stimulation of LH-projecting CRH^{PVN} neurons but not Hcrt neurons significantly increased wake amount. Absence of Hcrt neurons or CRISPR-Cas9–mediated disruption of *crh* gene in CRH^{PVN} neurons compromised this effect (Q, †$P < 0.0001$; R, †$P < 0.0001$; S, **$P = 0.0072$). (B to D, F to H, J to L, and N to P) Linear mixed-effects model followed by Šidák's multiple comparisons, dark phase indicated by gray shielding; (Q to S) one-way analysis of variance (ANOVA) followed by Šidák's multiple comparisons; *$P < 0.05$, ***$P < 0.005$, ****$P < 0.001$, †$P < 0.0005$; $n = 6$ mice for each group.

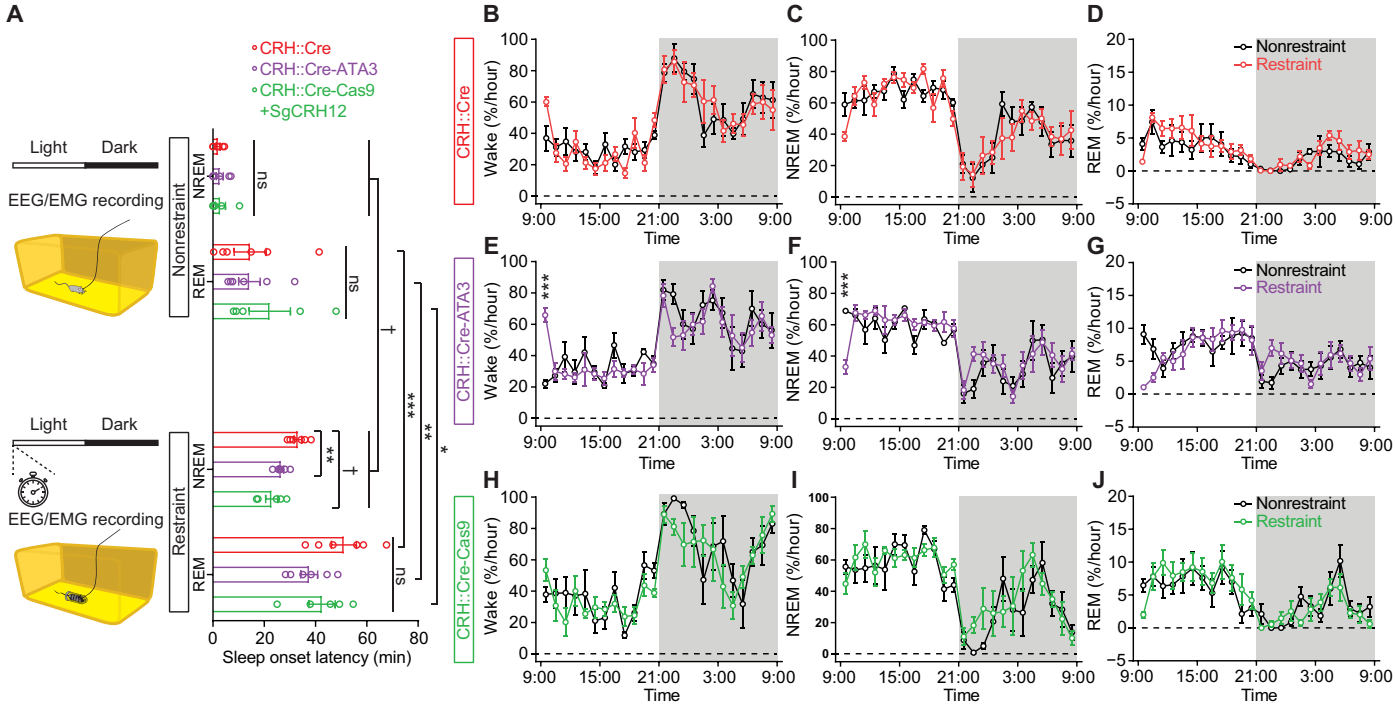

Fig. 5. Disruption of the CRH^{PVN}-Hcrt^{LH} circuitry significantly reduces the latency to NREM sleep onset following a 10-min restraint session without affecting the general sleep/wake pattern. (**A**) Absence of Hcrt neurons or disruption of *crh* gene in CRH^{PVN} neurons significantly reduced the latency to NREM sleep onset after a 10-min restraint stress session. (**B** to **J**) A 10-min restraint stress session did not alter the general sleep architecture of mice with intact (B to D) or disrupted CRH^{PVN}-Hcrt^{LH} circuitry (E to J). (A) One-way ANOVA followed by Šidák's multiple comparisons, paired *t* test between nonrestraint and restraint for a given genotype; (B to J) linear mixed-effects model followed by Šidák's multiple comparisons, dark phase indicated by gray shielding; **P* < 0.05, ***P* < 0.01, ****P* < 0.005, †*P* < 0.0005; *n* = 6 mice for CRE::Cre and CRH::Cre-ATA3, *n* = 5 for CRH::Cre-Cas9. ns, not significant.

components of both the innate and adaptive immune systems. CRH neuron stimulation may alter immune cell distribution through several mechanisms including alteration of intracellular signaling responses implicated in the mobilization, adhesion, proliferation, and survival of these cells (*36*).

We next investigated the effect of CRH^{PVN} neuron stimulation on the activity of key signaling pathways implicated in the immune response to stress, including elements of the nuclear factor κB (NFκB), mitogen-activated protein kinase (MAPK), and Janus kinase (JAK)/signal transducer and activator of transcription (STAT) signaling pathways. CRH neuron stimulation promoted expression of IκB (inhibitor of nuclear factor κB) in nearly all cell types examined (Fig. 6B, left panel, and fig. S8), consistent with the known inhibitory effects of glucocorticoids on NFκB signaling (*37*, *38*). In addition, optogenetic stimulation down-regulated pSTAT6 protein expression in many immune cell subsets, including B cells, CD4$^+$, and CD8$^+$ T cells, and NK cells, consistent with prior observations of direct interactions between the glucocorticoid receptor and STAT6 (*39*). The inhibition of NFκB and STAT6 signaling responses in T cells and monocyte subsets, as well as the observed reductions in the numbers of circulating CD4$^+$ T cells, B220$^+$ B cells, NK cells, and monocyte subsets suggest that CRH neuronal stimulation promoted widespread immunosuppression consistent with known glucocorticoid responses (*40*). Our observation of central optogenetically induced immunosuppression is consistent with an enhancement of glucocorticoid signaling by physical restraint stress as reported earlier (*41*). Therefore, we identified a neural substrate for stress-induced immunosuppression.

DISCUSSION

In this study, we find that the CRH^{PVN}-Hcrt^{LH} pathway plays a crucial role underlying stress-induced insomnia/hyperarousal and systemic immunosuppression. We showed that CRH^{PVN} neurons are sufficient but not necessary to trigger Hcrt^{LH} neuronal activity. We further demonstrated that optogenetic activation of CRH^{PVN} neurons projecting to the LH elicits long-lasting wakefulness mimicking insomnia/hyperarousal induced by stress exposure. We found that CRH release from PVN neurons is necessary for optogenetically evoked hyperarousal and restraint stress–induced insomnia. These observations are in line with earlier work showing that stress induces CRH release in the PVN (*42*), and knockdown of CRH attenuates stress-induced social avoidance (*43*). In addition, ablation of Hcrt neurons partially reduces the amount of wakefulness elicited by optogenetically stimulating CRH^{PVN} neurons projecting to LH and decreases the latency to NREM sleep onset following restraint stress. Our work highlights that the CRH^{PVN} signaling pathway is a prominent target for the treatment of insomnia/hyperarousal and stress-induced changes in systemic physiology.

Optical dissection of CRH^{PVN}-Hcrt^{LH} circuitry in insomnia induced by stress

cFos staining of brain slices following restraint stress informed us that the hyperactivities of CRH^{PVN} and Hcrt^{LH} neurons are potentially implicated in stress-induced insomnia pathology. Many brain nuclei including hypocretinergic (*5*), aminergic (*6*–*8*), and basal forebrain cholinergic neurons (*9*, *10*) are capable of switching arousal

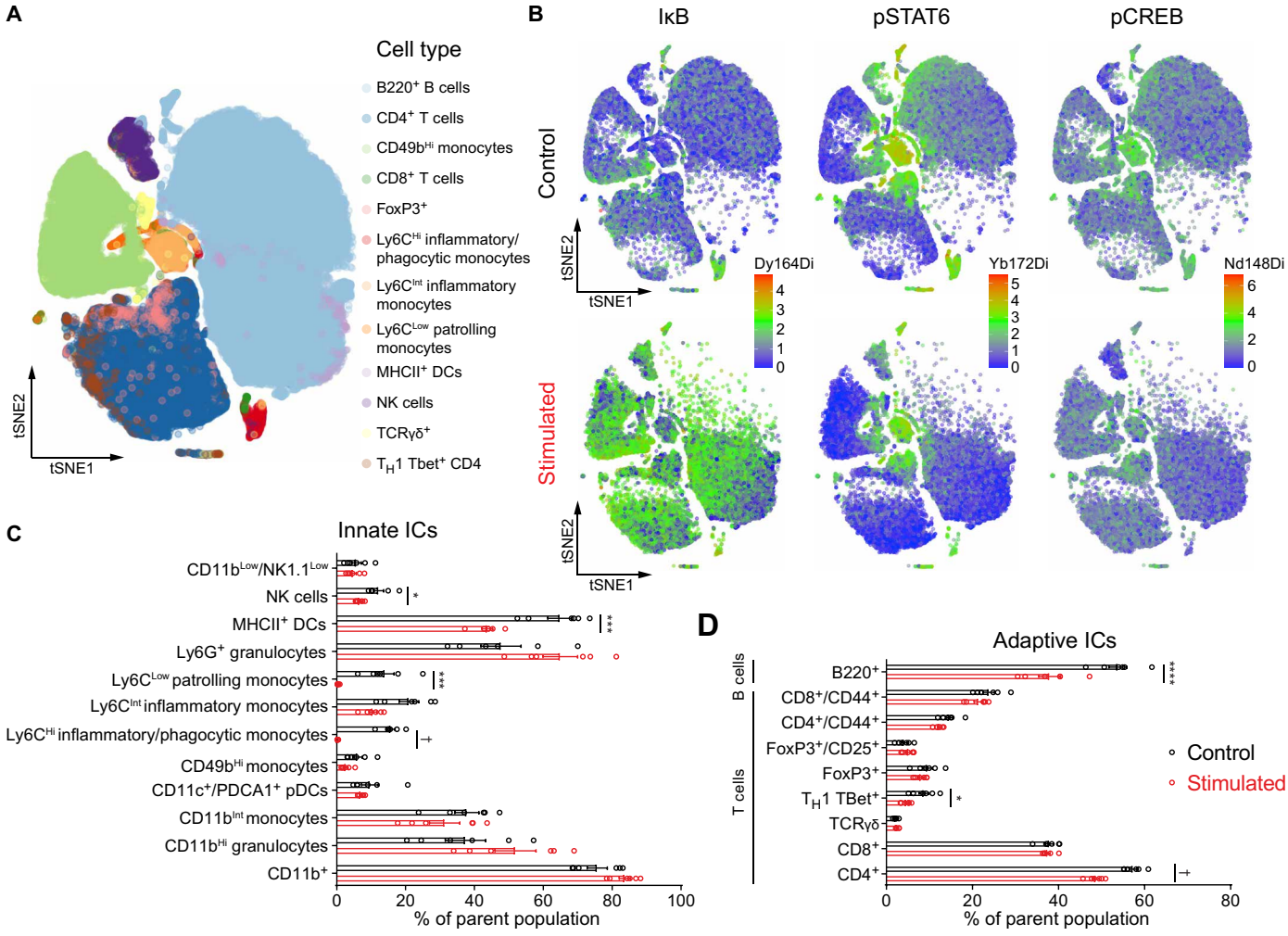

Fig. 6. CRH^{PVN} activation drives changes in systemic immunity consistent with immunosuppression. (**A**) Cell subpopulation distribution in the pooled dataset based on all samples. (**B**) Composite tSNE plots of intracellular protein expression from control and optogenetically stimulated mice for IκB (left), pSTAT6 (middle), and pCREB (right). (**C**) Distribution of circulating innate immune cells (ICs) at baseline (black bars) and in response to CRH neuronal stimulation (red bars), including NK1.1$^+$ NK cells, MHCII$^+$ dendritic cells, Ly6C^{Low} patrolling monocytes, and Ly6C^{Hi} inflammatory/phagocytic monocytes. (**D**) Distribution of circulating adaptive ICs at baseline (black bars) and in response to CRH neuronal stimulation (red bars), including B lymphocytes (B220$^+$), was decreased. T lymphocyte subsets altered include T$_H$1 TBet$^+$ cells and CD4$^+$ T cells. $n = 6$ mice per group, error bars represent SEM, Holm-Šidák test, *$P < 0.05$, ***$P < 0.005$, ****$P < 0.001$, †$P < 0.0005$.

states from sleep to wake. However, the optogenetic stimulation paradigms used in these experiments usually consist of multiple light pulses at frequencies mimicking or above their natural neuronal firing rates, and insomnia/hyperarousal has not been reported following optogenetic stimulation of these brain nuclei. Strong optogenetic stimulations (higher light intensity, higher frequencies, and multiple pulses/train) of Hcrt neurons reliably promote and consolidate wakefulness in Hcrt::Cre mice (*44*). To avoid a potential saturation of wakefulness by stimulating this circuitry, we used a mild stimulation paradigm (10-mW, 15-ms pulse at 0.1 Hz for 6 hours) to dissect either node of the CRH^{PVN}-Hcrt^{LH} pathway in sleep/wake regulation. Although this mild stimulation paradigm was insufficient to promote wakefulness in Hcrt::Cre mice, the same stimulation of CRH^{PVN} neurons projecting to LH where Hcrt neurons are located markedly elevated the arousal level mimicking insomnia under stress. Our observation is consistent with an earlier report showing that a single central administration of CRH causes long-lasting wakefulness (*30*). We further investigated the specific role of Hcrt neurons and the *crh* gene in CRH^{PVN} neurons in the same stimulation scenario. Genetic ablation of Hcrt neurons significantly reduced the wakefulness amount upon optogenetic stimulation of LH-projecting CRH^{PVN} neurons. The partial compromise of hyperarousal by genetic ablation of Hcrt neurons indicates CRH exerts arousal-promoting effect through other downstream neurons besides Hcrt^{LH} neurons. For example, activation of neurons expressing neurotensin intermingled with Hcrt neurons in the LH has been reported to increase wake amount (*45*). Notably, CRISPR-Cas9–mediated knockdown of the *crh* gene completely abolished the hyperarousal phenotype upon optogenetic stimulation of LH-projecting CRH^{PVN} neurons. These observations highlight that the hormone CRH plays a pivotal role in stress-induced insomnia/hyperarousal. Fiber photometry recording revealed CRH^{PVN} neurons are silent during natural sleep-to-wake

transitions, but highly active under stress. The concomitant $Hcrt^{LH}$ neuronal activity under stress suggests that CRH^{PVN} neurons recruit Hcrt neurons to mediate hyperarousal. The responses of $Hcrt^{LH}$ neurons to neutral/positive stimuli indicate that these neurons could be engaged in various conditions requiring vigilance independent of valence.

Neural substrates of stress-induced peripheral immunosuppression

An earlier study has linked the activation of reward-related VTA dopaminergic neurons to an enhancement of innate and adaptive immunity including elevated antibacterial activity of monocytes and macrophages (*46*). Reciprocally, stress-induced insomnia is often associated with deficits in immune function in humans (*47*). However, the neural substrates linking stress, arousal, and immunity are poorly understood. As we discussed above, CRH neurons in the PVN serve as a key node in the behavioral and physiological stress response in part via the promotion of downstream glucocorticoid secretion from the adrenal cortex. We identified the CRH^{PVN}-$Hcrt^{LH}$ pathway as a critical regulator coupling stress to arousal and protracted insomnia. A recent study showed that hypocretin-null mice developed monocytosis, whereas Hcrt supplementation decreased the concentration of $Ly6C^{Hi}$ monocytes (*48*) and therefore established a link between the hypocretinergic system and immune regulation. Our observation that stimulation of CRH^{PVN} soma resulted in dynamic changes in immune cell distribution and functional responses (e.g., reduction in circulating $CD4^+$ T cells and increases in IκB expression) is consistent with known immunosuppressive effects of glucocorticoids. Acute stress appears to prime immunity, whereas chronic stress usually suppresses immune function. Given a mild optogenetic stimulation of CRH^{PVN} neurons is sufficient to elicit insomnia/hyperarousal, a stronger stimulation paradigm that we used to study immune function likely overwhelmed the CRH^{PVN} circuitry, and thus mimicking the effect of chronic stress on immune function. Further studies are needed to understand how different stimulation paradigms influence systemic and tissue-specific immune cell populations.

An alternative explanation (beyond glucocorticoid up-regulation) for the changes we observed may depend on CRH^{PVN}-mediated activation of the sympathetic nervous system. CRH^{PVN} neurons drive downstream sympathetic activation via projections to the brainstem nucleus of the solitary tract (*49*). Postganglionic sympathetic nerves have well-known immunomodulatory effects, driven largely by the effect of their neurotransmitter product, norepinephrine (*49*). In early studies, the effects of CRH on the immune system appeared to be dependent on the sympathetic nervous system, as chemical sympathectomy and pharmacological blockade of β-adrenergic receptors reversed the observed effect of CRH on immune function (*50*). If the immunosuppressive phenotype we observed depends on sympathetic activation, then β-adrenergic blockade may additionally prevent immune dysfunction associated with stress and insomnia [e.g., as in (*51*)]. Recently, a study demonstrated that CRH^{PVN} neurons can influence the development and function of peripheral antibody–producing B cells (plasma cells) via their projections to the splenic nerve (*52*). Delineating how these neurons differentially promote enhancement of humoral immunity in one condition and elicit broad immunosuppression in another is still an open question that needs to be addressed.

Together, we reveal that the CRH^{PVN}-$Hcrt^{LH}$ pathway plays a critical role in hyperarousal via optical interrogation of sleep, and systemic immunity with CyTOF analysis of immune factors. Therefore, we identify a shared neural substrate for insomnia and immunosuppression under stress.

MATERIALS AND METHODS

Animals

Experiments were performed following the protocols approved by the Stanford University Animal Care and Use Committee in accordance with the National Institutes of Health *Guide for the Care and Use of Laboratory Animals*. Discomfort, distress, and pain were minimized with anesthesia and analgesic medications. Young adult (3 to 6 months) male mice were used in this study. Mice were housed in a temperature- and humidity-controlled animal facility with a 12-hour/12-hour light/dark cycle (9:00 light on, 21:00 light off). Standard laboratory mouse food pellets and water were available ad libitum. Hcrt-IRES-Cre knock-in heterozygotes (Hcrt::Cre) (*12*), Hcrt/orexin/ataxin-3 mice (ATA3) (*28*), and CRH::Cre [B6(Cg)-$Crh^{tm1(cre)Zjh}$/J, JAX stock no. 012704], AVP::Cre [B6.Cg-$Avp^{tm1.1(cre)Hze}$/J, JAX stock no. 023530], and OXT::Cre [B6;129S-$Oxt^{tm1.1(cre)Dolsn}$/J, JAX stock no. 024234] were backcrossed onto C57BL/J backgrounds. CRH::Cre-ATA3 mice were generated by crossing CRH::Cre heterozygotes with ATA3 heterozygotes. CRH::Cre-Cas9 mice were generated by crossing CRH::Cre heterozygotes with Cas9 homozygotes [B6J.129(B6N)-Gt(ROSA)26$Sor^{tm1(CAG-cas9*,-EGFP)Fezh}$/J, JAX stock no. 026175]. Vgat::Cre-tdTomato mice were generated by crossing Vgat::Cre [Slc32a1$^{tm2(cre)Lowl}$/J, stock no. 016962] heterozygotes with Ai 14 [B6;129S6-Gt(ROSA)26$Sor^{tm14(CAG-tdTomato)Hze}$/J, JAX stock no. 007908] homozygotes.

EEG/EMG electrode fabrication and implantation

Mini-screw (US Micro Screw) was soldered to one tip of an insulated mini wire with two tips exposed, and the other tip of the mini-wire was soldered to a golden pin aligned in an electrode socket. A mini-ring was made on one side of an insulated mini-wire with the other side soldered to a separate golden pin in the electrode socket. Each electrode socket contains four channels with two mini-screw channels for EEG recording and two mini-ring channels for EMG recording. The resistance of all the channels was controlled with a digital multimeter (Fluke) lower than 1.5 ohms for ideal conductance. Mice were mounted onto an animal stereotaxic frame (David Kopf Instruments) under anesthesia with a mixture of ketamine (100 mg/kg) and xylazine (20 mg/kg). Two mini-screws were placed in the skull above the frontal [anteroposterior (AP), −2 mm; mediolateral (ML), ±1 mm] and temporal (AP, 3 mm; ML, ±2.5 mm) cortices for sampling EEG signals, and two mini-rings were placed in the neck muscles for EMG signal acquisition. Electrode sockets were secured with Metabond and dental acrylic on the skull for recording in freely moving mice. After surgery, mice were administered with buprenorphine-SR (0.5 mg/kg; 30 min before and 24 to 48 hours after surgery, subcutaneously) for pain relief.

EEG/EMG recording and analysis

EEG/EMG signals were sampled at 256 Hz with VitalRecorder (Kissei Comtec Co.) following amplification through an amplifier with multiple channels (Grass Instruments). The band-pass was set between 0.1 and 120 Hz. Raw EEG/EMG data were exported to MATLAB (MathWorks, Natick, MA, USA) and analyzed with custom scripts and MATLAB built-in tools based on described criteria (*5*) to determine

behavioral states. For optogenetic and fiber photometry recording experiments, simultaneous EEG/EMG signals were recorded to determine behavioral states. The raw EEG/EMG signals with/without GCaMP6f traces were imported to MATLAB for offline analysis.

Virus injection and fiber optic implantation

Monosynaptic tracing of inputs to Hcrt^{LH} neurons

To determine the cell type in the PVN with direct innervation of Hcrt^{LH} neurons, we used the EnvA-pseudotyped glycoprotein (G)–deleted rabies virus (EnvA + RV*d*G) tracing strategy (*21*). First, a mixture of AAV-5 EF1α-Flex TVA-mCherry (AAV67, lot no. 388b, 2.5×10^{12} gc/ml (genome copies/ml), Stanford virus core) and AAV-8(Y733F)-CAG Flex RabiesG (AAV-59, lot no. 1489, 5.0×10^{13} gc/ml, Stanford virus core) was injected to the LH of young (3 to 6 months) male Hcrt::Cre mice to target the Hcrt field [AP, −1.35 mm; ML, ±0.95 mm; dorsoventral (DV), −4.85 to DV, −5.15 mm) under anesthesia and analgesic as described above. Two weeks later, the same mice were injected with EnvA G-deleted rabies green fluorescent protein (GFP) (6.04×10^{7} gc/ml, Salk Institute Gene Transfer Targeting and Therapeutics Core) at the coordinates same with the first injection. One week after the second injection, colchicine (1.0 μl of 7 μg/ml solution per hemisphere, for PVN CRH/AVP/OXT neuropeptide immunostaining) was injected to the lateral ventricles (AP, −0.65 mm; ML, ±0.95 mm; DV, −2.55 mm) under anesthetics and analgesic as described above. Then, mice were anesthetized and perfused 24 to 48 hours later for immunostaining.

AAV-retro tracing of LH upstream neurons

PVN is known as a hub containing intermingled CRH, AVP, and OXT neurons (*19*). To further validate that the LH receives neuronal projections from PVN, we injected AAV-Retro-EF1α-DIO-hChR2 (C128S/D156A)-eYFP (AAV-Retro, Stanford Virus Core, 3.3×10^{13} gc/ml, lot no. 3908) to the LH containing Hcrt field (AP, −1.35 mm; ML, ±0.95 mm; DV, −5.15 mm) of young male CRH::Cre, AVP::Cre, OXT::Cre mice, respectively, under anesthetics and analgesic as aforementioned. Three weeks after injection, colchicine (1.0 μl of 7 μg/ml solution per hemisphere, for PVN CRH/AVP/OXT neuropeptide immunostaining) was injected to the lateral ventricles (AP, −0.65 mm; ML, ±0.95 mm; DV, −2.55 mm). Then, mice were anesthetized and perfused 24 to 48 hours later for immunostaining.

Fiber photometry

For fiber photometry recording from Hcrt^{LH} [also known as orexin (*53*, *54*)] neurons in Hcrt::Cre mice, 0.3 μl of AAV vectors carrying genes encoding GCaMP6f (AAV-DJ-EF1α-DIO-GCaMP6f, 1.1×10^{12} gc/ml, Stanford Virus Core, lot no. 3725) was delivered to left (L)/right (R) LH (AP, −1.35 mm; ML, ±0.95 mm; DV, −5.15 mm) of young male Hcrt::Cre mice with a 5-μl Hamilton microsyringe, and a glass fiber (400-μm core diameter, Doric Lenses) was implanted with the tip at the injection site for GCaMP6f signal acquisition later on. For recording from CRH^{PVN} neurons, the same virus was injected to L/R PVN (AP, −0.90 mm; ML, ±0.30 mm; DV, −4.66 mm), and glass fiber was placed at the same site of young CRH::Cre mice. EEG and EMG electrodes were implanted after securing the fiber optic with meta-bond and dental acrylic. Mice were housed in their home cages to recover for at least 2 weeks to get sufficient viral expression before connection to the EEG/EMG recording cables and fiber photometry recording patch cord.

Optogenetic experiments

For optogenetic experiments, 0.3 μl of AAV-DJ-EF1α-DIO-hChR2(H134R)-eYFP viruses (ChR2-eYFP, 6.5×10^{12} gc/ml, Stanford Virus Core, lot no. 4176) was delivered to LH (AP, −1.35 mm; ML, ±0.95 mm; DV, −5.15 mm) of anesthetized young (3 to 6 months) male Hcrt::Cre mice according to stereotaxic coordinates determined on Kopf stereotaxic frame with a 5-μl Hamilton microsyringe. A glass fiber (200-μm core diameter, Doric Lenses, Franquet, Québec, Canada) was implanted with the tip right above the injection site for optogenetic stimulations later on. For stimulating CRH^{PVN} neurons projecting to LH, AAV-Retro-EF1α-DIO-hChR2(C128S/D156A)-eYFP (AAV-Retro, Stanford Virus Core, 3.3×10^{13} gc/ml, lot no. 3908) was injected to LH with the same coordinates for Hcrt::Cre mice. A glass fiber (200-μm core diameter, Doric Lenses, Franquet, Québec, Canada) was implanted with the tip right above the CRH^{PVN} neurons (AP, −0.90 mm; ML, ±0.30 mm; DV, −4.3 mm) for optogenetic stimulations of LH-projecting CRH^{PVN} neurons later on. After fixation of glass fiber and EEG/EMG electrode implantation, mice were allowed to recover for at least 2 weeks to get sufficient viral expression before connecting to the EEG/EMG recording cables and optical stimulation patch cord.

CRISPR-Cas9–mediated *crh* gene disruption in CRH::Cre-Cas9 mice

Crh gene target sites for CRISPR-Cas9 were designed by CHOPCHOP (http://chopchop.cbu.uib.no) (*55*). The target sequences were as follows: sgCRH1, 5′-ATGCGGATCAGAACCGGCTG-3′; sgCRH2, 5′-CAACTCCACGCCCCTCACCG-3′. Oligonucleotides encoding guide sequences are purchased from Integrated DNA Technologies (IDT) and cloned individually into the Bbs I fragment of pX458 [Addgene plasmid 48138 (*56*)]. U6-sgCRH1and U6-sgCRH2 fragments were polymerase chain reaction amplified, respectively, using pX458-sgCRH as a template. Amplified fragments were cloned tandemly into Mlu I–digested pAAV-EF1α-DIO-mCherry (Addgene plasmid 20299) by Gibson assembly method. The primers used were as follows: Gibson1-F, 5′-TAGGGGTTCCTGCGGCCGCAGAGGGCCTATTTCCCATG-3′; Gibson1-R, 5′-ATAGGCCCTCGGTACCAAAAATCTCGCC-3′; Gibson2-F, 5′-TTTTTCTAGAGAGGGCCTATTTCCCATG-3′; Gibson2-R, 5′-ATCCATCTTTGCAAAGCTTAAAAAATCTCGCCAACAAGTTG-3′. AAV constructs carrying nontargeting guide sequences were used as control (*29*). pAAV-U6-sgCRH1-U6-sgCRH2-EF1α-DIO-mCherry and pAAV-U6-sgControl-U6-sgControl-EF1α-DIO-mCherry were packaged into AAV-DJ by the gene vector and virus core at Stanford University. AAV-DJ-U6-sgControl-EF1α-DIO-mCherry (0.6 μl) (5×10^{12} gc/ml, lot no. 4354) and AAV-DJ-U6-sgCRH12-EF1α-DIO-mCherry viruses (3×10^{12} gc/ml, lot no. 4553) were respectively injected to PVN (AP, −0.90 mm; ML, ±0.30 mm; DV, −4.5 + −4.8 mm; 0.3 μl each depth) unilaterally of the CRH::Cre-Cas9 mice for *crh* gene disruption validation. Three weeks after the virus injection, colchicine (1.0 μl of 7 μg/ml solution per hemisphere, for CRH neuropeptide immunostaining) was injected to the lateral ventricles (AP, −0.65 mm; ML, ±0.95 mm; DV, −2.55 mm). Then, mice were anesthetized and perfused 24 to 48 hours later for immunostaining. For optogenetic stimulation of LH-projecting CRH^{PVN} neurons with *crh* gene disrupted, 0.6 μl of AAV-DJ-U6-sgCRH12-EF1α-DIO-mCherry viruses was injected to the L/R PVN (−0.90 mm; ML, ±0.30 mm; DV, −4.5 + −4.8 mm; 0.3 μl each depth) unilaterally of CRH::Cre-Cas9 mice under anesthesia, and 0.3 μl of AAV-Retro-EF1α-DIO-hChR2(C128S/D156A)-eYFP viruses was injected to the LH (AP, −1.35 mm; ML, ±0.95 mm; DV, −5.15 mm) of the same hemisphere. Afterward, a glass fiber (200-μm core diameter, Doric Lenses)

targeting PVN infected by viral vectors was implanted for optogenetic stimulation of *crh* gene ablated CRH^{PVN} neurons projecting to LH, and EEG/EMG electrodes were implanted for EEG/EMG recording later on. For the restraint stress on sleep experiment, 0.6 μl of AAV-DJ-U6-sgCRH12-EF1α-DIO-mCherry viruses was injected to the PVN (−0.90 mm; ML, ±0.30 mm; DV, −4.5 + −4.8 mm; 0.3 μl each depth) bilaterally of CRH::Cre-Cas9 mice under anesthesia, and EEG/EMG electrodes were implanted for sleep pattern recording afterward.

Restraint stress and sleep recording

A well-established noninvasive restraint paradigm was used to generate acute stress in mice (*18*). For the cFos immunostaining experiment, nine young adult male wild-type (WT) mice (3 to 5 months) were individually placed head first into a well-ventilated 50-ml Falcon conical tube with a narrow open window on top placed in their home cages. After a 10-min restraint session, mice were immediately released from the restraint tubes. Mice were randomly separated into three groups and were perfused at 20 min (n = 3), 80 min (n = 3), and 140 min (n = 3) after the restraint stress termination. For evaluating the impact of restraint stress on latency to sleep onset and general sleep architecture, young adult male mice (3 to 6 months, CRH::Cre, CRH::Cre-ATA3, CRH::Cre-Cas9 infused with *crh* gene disrupted bilaterally in CRH^{PVN} neurons) with EEG/EMG implants (for sleep pattern monitoring) were exposed to the restraint tubes with a narrow window on top for EEG/EMG cable sliding. During the entire restraint procedure, mice were in a natural body position without physical harm in their home cages. The restraint stress lasted for 10 min at the beginning of the light phase when mice have a strong drive for sleep. EEG/EMG signals were recorded starting from the onset of restraint stress. Mice were released from the restraint tubes immediately after a 10-min restraint session.

Salient stimuli

GCaMP6f signal was recorded from CRH^{PVN} neurons in male CRH::Cre mice and from $Hcrt^{LH}$ neurons in male Hcrt::Cre mice housed individually with 1-week habituation to fiber patch cord. GCaMP6f signal was sampled for 4 min each session with 2 min as baseline and 2-min exposure to salient stimuli including a 15-ml novel Falcon tube (novelty), novel male mouse, novel female mouse, HFD (in a small petri dish), rat bedding (in a small petri dish), restraint (mouse placed in a well-ventilated 50-ml Falcon conical tube with a narrow window for fiber patch cord sliding), TMT (a small piece of filtration paper with 5-μl TMT in a small petri dish), and manual grabbing. For the EPM open arm exposure, mouse was transferred from the home cage onto the open arm of the EPM with the entrance to EPM center blocked. Salient stimuli were removed immediately from the mice after 2 min. Introduction of salient stimuli to each individual mouse was randomly shuffled.

Fiber photometry signal acquisition and analysis

Following recovery and habituation to EEG/EMG cable lead and fiber optic patch cord (400-μm core diameter, Doric Lenses), mice expressing Cre-dependent GCaMP6f were connected to EEG/EMG recording setup and custom-built fiber photometry setup (*44*), respectively. Briefly, a 470-nm light-emitting diode (LED) (M470D3, Thorlabs, NJ, USA) was sinusoidally modulated at 211 Hz and passed through a GFP excitation filter followed by a dichroic mirror (MD 498, Thorlabs) for reflection. The light stream was sent through a high numerical aperture (NA) (0.48), large core (400 μm) optical fiber patch cord (Doric Lenses, Québec, Canada), which was connected with a zirconia connector (Doric Lenses, Québec, Canada) to the dental acrylic–secured fiber optic implant (0.48 NA, 400 μm, Doric Lenses, Québec, Canada) with the tip above the injection site targeting CRH^{PVN} or $Hcrt^{LH}$ neurons. Separately, a 405-nm LED was modulated at 531 Hz and filtered by a 405-nm band-pass filter and sent through the optical fiber patch cord to mouse brain to evoke reference fluorescence, which is independent of Ca^{2+} release. GCaMP6f fluorescence and reference fluorescence were sampled by the same fiber patch cord through a GFP emission filter (MF525-39, Thorlabs), and center aligned to a photodetector (Model 2151, Newport, Irvine, CA, USA) with a lens (LA1540-A, Thorlabs). The analog signals were amplified by two lock-in amplifiers for GFP fluorescence and reference fluorescence, respectively (model SR380, Stanford Research Systems, Sunnyvale, CA, USA). MATLAB-based custom software was used to control the LEDs and sample both the GFP fluorescence and reference fluorescence through a multifunction data acquisition device (National Instruments, Austin, TX, USA) with 256-Hz sampling frequency in a real-time manner. $\Delta F/F$ was obtained by subtracting the reference fluorescence signal from the 470-nm excited GFP emission signal to remove the system interference. GCaMP6f from CRH^{PVN} or $Hcrt^{LH}$ neurons, and simultaneous EEG/EMG recordings were conducted between 14:00 and 18:00 during the light phase. GCaMP6f signals were staged to different behavioral state transitions based on the simultaneously recorded EEG/EMG signals. The behavioral state transition category includes NREM to brief wake, NREM to REM, NREM to long wake, REM to brief wake, REM to long wake, and wake to NREM. Traces for each behavioral state transition were plotted with transition time point defined as 0 for CRH::Cre and Hcrt::Cre mice. For GCaMP recording during salient stimuli challenges, time of introduction of the stimuli to the mice was defined as time 0. A z score was calculated by subtracting the mean value of GCaMP6f after time 0 from the mean value of GCaMP6f trace before time 0.

Optogenetic stimulation

After recovery, mice injected with viruses expressing Cre-dependent ChR2-eYFP were connected to EEG/EMG recording cables and fiber optic patch cord (200-μm core diameter, Doric Lenses) for 1-week acclimation in cages with open top, which allowed mice to move freely. Following acclimation, EEG and EMG were recorded for 24 hours covering an entire light/dark cycle with 15-ms 10-mW (Laserglow, calibrated with Thorlabs light meter) 473-nm light pulse optogenetic stimulation at 0.1 Hz for 6 hours starting from the beginning of the light phase.

Histology

For in vivo experiments, upon accomplishment of recordings, mice were perfused under anesthesia (100 mg/kg ketamine and 20 mg/kg xylazine mixture) with ice-cold 1× phosphate-buffered saline (PBS) to verify the viral expression and glass fiber placement. Brains were rapidly extracted, postfixed with 4% paraformaldehyde (PFA) at 4°C overnight, and equilibrated in 30% sucrose in PBS containing 0.1% NaN_3. Then, brains were sectioned at −22°C with a cryostat (Leica Microsystems) at a thickness of 35 μm. Slices were collected from anterior to posterior consecutively to 24-well plates containing 1× PBS with 0.1% NaN_3, covered with aluminum foil, and stored at 4°C until immunostaining and imaging. Primary polyclonal antibody against OX-A/Hcrt-1 [SC-8070, lot no. A2915, goat polyclonal

immunoglobulin G (IgG)] and primary polyclonal antibodies against cFos (host: rabbit, catalog no. SC-52, lot no. J0815; host: goat, catalog no. SC-52-G, lot no. F1716) were purchased from Santa Cruz Biotechnology, INC. Primary polyclonal antibody against cFos (host: rabbit, catalog no. 26209, lot no. 1714001), primary polyclonal antibody against CRH (host: rabbit, catalog no. 20084, lot no. 533038), primary polyclonal antibody against AVP (host: rabbit, catalog no. 20069, lot no. 1911001), and primary polyclonal antibody against OXT (host: rabbit, catalog no. 20068, lot no. 1607001) were purchased from ImmunoStar. Secondary antibodies Alexa Fluor 594 Donkey anti-goat IgG (H + L, catalog no. A-11058), Alexa Fluor 594 donkey anti-rabbit IgG (H + L, catalog no. A32754), Alexa Fluor 488 donkey anti-rabbit IgG (H + L, catalog no. A-21206), and Alexa Fluor 647 donkey anti-rabbit IgG (H + L, catalog no. A-31573) were purchased from Invitrogen (manufacturer: Life Technologies). Appropriate antibodies were selected for staining depending on the experimental paradigms. For the WT mice used for restraint stress, sections around PVN and LH were washed in 1× PBS for 5 min, three times, and incubated in a blocking solution of 1× PBS with 0.3% Triton X-100 (PBST) and 4% bovine serum albumin for 1 hour. Following that, CRH primary antibody and OX-A/Hcrt-1 primary antibody were added to the wells containing slices around PVN and wells containing LH slices, respectively, and cFos primary antibody was added to both PVN slice–containing wells and LH slice–containing wells with blocking solution (1:800) overnight. On the second day, sections were washed in 1× PBS for 5 min, three times, and incubated in blocking buffer for 2 hours. After blocking, secondary antibody was added to the blocking buffer for 2 hours (dilution 1:800). After three times of 5-min 1× PBS washing, brain sections were mounted onto gelatin-coated slides, covered with Fluoroshield containing 4′,6-diamidino-2-phenylindole Mounting Media (Sigma-Aldrich, F6057) and coverglass for imaging with a widefield microscope (Zeiss AxioImager, Germany) for the entire section or LSM710 confocal microscope for enlarged visualization (Zeiss, Germany). For cell type determination in PVN of Vgat::Cre-Ai14 mice, colchicine (1.0 μl of 7 μg/ml solution per hemisphere, for PVN CRH/AVP/OXT neuropeptide staining) was injected to the lateral ventricles (AP, −0.65 mm; ML, ±0.95 mm; DV, −2.55 mm). Then, mice were anesthetized and perfused within 24 to 48 hours for immunostaining.

Mass cytometry by time of flight

CRH::Cre mice were equipped with EEG/EMG electrodes as described previously. AAVs encoding the optogenetic actuator ChR2 (AAV-DJ-DIO-EF1α-ChR2-eYFP; lot no. 5227; 4.12×10^{12} gc/ml) were infused into the paraventricular nucleus [unilateral; 0.4 μl; AP, −0.90 mm; ML, ±0.25 mm; DV, −4.85 mm (injection); DV, −4.6 mm (optic fiber)] over the course of 3 min followed by 10 min for viral distribution to the tissue. Then, a fiber optic implant (200-μm diameter, 5.5-mm length, Doric Lenses Inc.) was slowly lowered and cemented in place above the PVN. Mice were allowed to recover for at least 3 weeks before starting the experiment.

Following recovery, 15-ms 10-mW (Laserglow, calibrated with Thorlabs light meter) 473-nm light pulses at 10 Hz (10 s on, 20 s off) were delivered to the PVN for 1 hour, and then, whole blood was collected 3 hours following the start of stimulation using microcapillary tubes (retro-orbital bleed; approximately 350 μl of blood). Blood was immediately stabilized using a protein stabilization reagent, allowed to sit for 10 min and then placed at −80°C in cryovials until further processing. Red blood cells (RBCs) were lysed using 1× thaw-lyse buffer (Smart Tube Inc., San Carlos, CA) in ddH_2O. After lysing, cells were pelleted at 600*g* for 5 min at room temperature (RT). RBC-depleted samples were barcoded using palladium isotopes. In brief, cells were washed with cell staining media (CSM), 1× PBS, and 1× PBS containing 0.02% saponin and then placed into a deep well block. Unique barcoding reagents were added to each well of the block containing cells from each mouse and incubated for 15 min at RT. After incubation, cells were washed with CSM and then resuspended via brief vortexing. Then, all samples were pooled into a single fluorescence-activated cell sorting (FACS) tube for the next staining step. After washing and pelleting the pooled cells, 150 μl of Fc block was added, and cells were incubated at RT with gentle shaking (600 rpm) for 10 min. Then, 300 μl of the surface antibody mix (see table S1) was added, and cells were incubated at RT for 30 min with gentle shaking. Then, cells were washed, pelleted, and the supernatant was collected and discarded. To permeabilize cells for intracellular staining, 700 μl of MeOH was added to the tube, and cells were incubated at 4°C for 10 min. Then, cells were washed with 1× PBS and CSM, followed by incubation with the intracellular antibody mix (see table S1) for 30 min at RT with gentle shaking (600 rpm). Cells were washed and then a DNA intercalator (DVS # Inter-1X-natir) was added in a mixture of 16% PFA/PBS. This mixture was incubated at 4°C overnight.

On the following day, the pooled sample was washed and then 1× normalization "beta" beads were added and cells were strained into a new FACS tube. Cells were run on a Helios (Fluidigm) machine using the SuperSampler attachment. Following the run, the data were normalized to the normalization bead signal. Then, data were run through de-barcoder software (MATLAB; bead distance 0.2) and individual .FCS files were gated and analyzed manually using ImmuneAtlas and Cytobank platforms. T-distributed stochastic neighbor embedding (tSNE) plots were generated for filtered singlet/leukocyte (i.e., RBCs excluded) populations for each file and formed into a composite plot. In brief, .FCS files were arcsinh transformed ($a = 0$, $b = 1/5$, $c = 0$), and 3000 randomly selected events were sampled for each file. T-distributed stochastic neighbor embedding (tSNE) was computed on the aggregated matrix with all events ($3000 \times 12 = 36{,}000$). The following parameters were used for tSNE in the RTsne package (https://CRAN.R-project.org/package=Rtsne): perplexity = 30, max_iter = 500. Then, the transformed coordinate events were mapped back to the sample they came from, as well as composite maps for each condition and the total population.

Statistical analysis

Hourly based sleep comparisons were analyzed by a linear mixed-effects model followed by Šidák's multiple comparisons as described in a similar counterbalanced crossover design (*44*). One-way analysis of variance (ANOVA) followed by Šidák's multiple comparisons was used to analyze alteration of sleep/wake amount for different experimental paradigms, and latency to sleep onset. Paired Student's *t* test was used for sleep/wake amount comparison between non-stim/nonrestraint and stim/restraint datasets. CyTOF data were analyzed with the Holm-Šidák test. In the figures, *, **, ***, ****, and † indicate $P < 0.05$, $P < 0.01$, $P < 0.005$, $P < 0.001$, and $P < 0.0005$, respectively. All values were reported as means ± SEM.

SUPPLEMENTARY MATERIALS

Supplementary material for this article is available at http://advances.sciencemag.org/cgi/content/full/6/37/eabc2590/DC1

View/request a protocol for this paper from *Bio-protocol*.

REFERENCES AND NOTES

1. T. L. Sterley, D. Baimoukhametova, T. Füzesi, A. A. Zurek, N. Daviu, N. P. Rasiah, D. Rosenegger, J. S. Bains, Social transmission and buffering of synaptic changes after stress. *Nat. Neurosci.* **21**, 393–403 (2018).
2. G. Cano, T. Mochizuki, C. B. Saper, Neural circuitry of stress-induced insomnia in rats. *J. Neurosci.* **28**, 10167–10184 (2008).
3. J. N. Morey, I. A. Boggero, A. B. Scott, S. C. Segerstrom, Current directions in stress and human immune function. *Curr. Opin. Psychol.* **5**, 13–17 (2015).
4. A. N. Vgontzas, E. O. Bixler, H. M. Lin, P. Prolo, G. Mastorakos, A. Vela-Bueno, A. Kales, G. P. Chrousos, Chronic insomnia is associated with nyctohemeral activation of the hypothalamic-pituitary-adrenal axis: Clinical implications. *J. Clin. Endocrinol. Metab.* **86**, 3787–3794 (2001).
5. A. R. Adamantidis, F. Zhang, A. M. Aravanis, K. Deisseroth, L. de Lecea, Neural substrates of awakening probed with optogenetic control of hypocretin neurons. *Nature* **450**, 420–424 (2007).
6. M. E. Carter, O. Yizhar, S. Chikahisa, H. Nguyen, A. Adamantidis, S. Nishino, K. Deisseroth, L. de Lecea, Tuning arousal with optogenetic modulation of locus coeruleus neurons. *Nat. Neurosci.* **13**, 1526–1533 (2010).
7. A. Eban-Rothschild, G. Rothschild, W. J. Giardino, J. R. Jones, L. de Lecea, VTA dopaminergic neurons regulate ethologically relevant sleep-wake behaviors. *Nat. Neurosci.* **19**, 1356–1366 (2016).
8. J. R. Cho, J. B. Treweek, J. E. Robinson, C. Xiao, L. R. Bremner, A. Greenbaum, V. Gradinaru, Dorsal raphe dopamine neurons modulate arousal and promote wakefulness by salient stimuli. *Neuron* **94**, 1205–1219.e8 (2017).
9. M. Xu, S. Chung, S. Zhang, P. Zhong, C. Ma, W. C. Chang, B. Weissbourd, N. Sakai, L. Luo, S. Nishino, Y. Dan, Basal forebrain circuit for sleep-wake control. *Nat. Neurosci.* **18**, 1641–1647 (2015).
10. S. O. Irmak, L. de Lecea, Basal forebrain cholinergic modulation of sleep transitions. *Sleep* **37**, 1941–1951 (2014).
11. Y. Yuan, W. Wu, M. Chen, F. Cai, C. Fan, W. Shen, W. Sun, J. Hu, Reward inhibits paraventricular CRH neurons to relieve stress. *Curr. Biol.* **29**, 1243–1251.e4 (2019).
12. W. J. Giardino, A. Eban-Rothschild, D. J. Christoffel, S.-B. Li, R. C. Malenka, L. de Lecea, Parallel circuits from the bed nuclei of stria terminalis to the lateral hypothalamus drive opposing emotional states. *Nat. Neurosci.* **21**, 1084–1095 (2018).
13. S. C. Segerstrom, G. E. Miller, Psychological stress and the human immune system: A meta-analytic study of 30 years of inquiry. *Psychol. Bull.* **130**, 601–630 (2004).
14. J. K. Kiecolt-Glaser, J. R. Dura, C. E. Speicher, O. J. Trask, R. Glaser, Spousal caregivers of dementia victims: Longitudinal changes in immunity and health. *Psychosom. Med.* **53**, 345–362 (1991).
15. K. Mizobe, K. Kishihara, R. Ezz-Din el-Naggar, G. A. Madkour, C. Kubo, K. Nomoto, Restraint stress-induced elevation of endogenous glucocorticoid suppresses migration of granulocytes and macrophages to an inflammatory locus. *J. Neuroimmunol.* **73**, 81–89 (1997).
16. D. W. Cain, J. A. Cidlowski, Immune regulation by glucocorticoids. *Nat. Rev. Immunol.* **17**, 233–247 (2017).
17. J. Minkel, M. Moreta, J. Muto, O. Htaik, C. Jones, M. Basner, D. Dinges, Sleep deprivation potentiates HPA axis stress reactivity in healthy adults. *Health Psychol.* **33**, 1430–1434 (2014).
18. A. Zimprich, L. Garrett, J. M. Deussing, C. T. Wotjak, H. Fuchs, V. Gailus-Durner, M. H. de Angelis, W. Wurst, S. M. Hölter, A robust and reliable non-invasive test for stress responsivity in mice. *Front. Behav. Neurosci.* **8**, 125 (2014).
19. A. Ramot, Z. Jiang, J. B. Tian, T. Nahum, Y. Kuperman, N. Justice, A. Chen, Hypothalamic CRFR1 is essential for HPA axis regulation following chronic stress. *Nat. Neurosci.* **20**, 385–388 (2017).
20. Y. C. Saito, T. Maejima, M. Nishitani, E. Hasegawa, Y. Yanagawa, M. Mieda, T. Sakurai, Monoamines inhibit GABAergic neurons in ventrolateral preoptic area that make direct synaptic connections to hypothalamic arousal neurons. *J. Neurosci.* **38**, 6366–6378 (2018).
21. E. M. Callaway, L. Luo, Monosynaptic circuit tracing with glycoprotein-deleted rabies viruses. *J. Neurosci.* **35**, 8979–8985 (2015).
22. D. G. Tervo, B.-Y. Hwang, S. Viswanathan, T. Gaj, M. Lavzin, K. D. Ritola, S. Lindo, S. Michael, E. Kuleshova, D. Ojala, C.-C. Huang, C. R. Gerfen, J. Schiller, J. T. Dudman, A. W. Hantman, L. L. Looger, D. V. Schaffer, A. Y. Karpova, A Designer AAV variant permits efficient retrograde access to projection neurons. *Neuron* **92**, 372–382 (2016).
23. H. S. Knobloch, A. Charlet, L. C. Hoffmann, M. Eliava, S. Khrulev, A. H. Cetin, P. Osten, M. K. Schwarz, P. H. Seeburg, R. Stoop, V. Grinevich, Evoked axonal oxytocin release in the central amygdala attenuates fear response. *Neuron* **73**, 553–566 (2012).
24. M. G. Lee, O. K. Hassani, B. E. Jones, Discharge of identified orexin/hypocretin neurons across the sleep-waking cycle. *J. Neurosci.* **25**, 6716–6720 (2005).
25. B. Y. Mileykovskiy, L. I. Kiyashchenko, J. M. Siegel, Behavioral correlates of activity in identified hypocretin/orexin neurons. *Neuron* **46**, 787–798 (2005).
26. J. Kim, S. Lee, Y. Y. Fang, A. Shin, S. Park, K. Hashikawa, S. Bhat, D. Kim, J. W. Sohn, D. Lin, G. S. B. Suh, Rapid, biphasic CRF neuronal responses encode positive and negative valence. *Nat. Neurosci.* **22**, 576–585 (2019).
27. J. S. Kim, S. Y. Han, K. J. Iremonger, Stress experience and hormone feedback tune distinct components of hypothalamic CRH neuron activity. *Nat. Commun.* **10**, 5696 (2019).
28. J. Hara, C. T. Beuckmann, T. Nambu, J. T. Willie, R. M. Chemelli, C. M. Sinton, F. Sugiyama, K. I. Yagami, K. Goto, M. Yanagisawa, T. Sakurai, Genetic ablation of orexin neurons in mice results in narcolepsy, hypophagia, and obesity. *Neuron* **30**, 345–354 (2001).
29. H. Yamaguchi, F. W. Hopf, S. B. Li, L. de Lecea, In vivo cell type-specific CRISPR knockdown of dopamine beta hydroxylase reduces locus coeruleus evoked wakefulness. *Nat. Commun.* **9**, 5211 (2018).
30. C. P. Romanowski, T. Fenzl, C. Flachskamm, W. Wurst, F. Holsboer, J. M. Deussing, M. Kimura, Central deficiency of corticotropin-releasing hormone receptor type 1 (CRH-R1) abolishes effects of CRH on NREM but not on REM sleep in mice. *Sleep* **33**, 427–436 (2010).
31. R. Winsky-Sommerer, A. Yamanaka, S. Diano, E. Borok, A. J. Roberts, T. Sakurai, T. S. Kilduff, T. L. Horvath, L. de Lecea, Interaction between the corticotropin-releasing factor system and hypocretins (Orexins): A novel circuit mediating stress response. *J. Neurosci.* **24**, 11439–11448 (2004).
32. R. Chen, X. Wu, L. Jiang, Y. Zhang, Single-cell RNA-seq reveals hypothalamic cell diversity. *Cell Rep.* **18**, 3227–3241 (2017).
33. J. Dabrowska, R. Hazra, J. D. Guo, S. Dewitt, D. G. Rainnie, Central CRF neurons are not created equal: Phenotypic differences in CRF-containing neurons of the rat paraventricular hypothalamus and the bed nucleus of the stria terminalis. *Front. Neurosci.* **7**, 156 (2013).
34. M. Mieda, J. T. Willie, J. Hara, C. M. Sinton, T. Sakurai, M. Yanagisawa, Orexin peptides prevent cataplexy and improve wakefulness in an orexin neuron-ablated model of narcolepsy in mice. *Proc. Natl. Acad. Sci. U.S.A.* **101**, 4649–4654 (2004).
35. S. C. Bendall, E. F. Simonds, P. Qiu, E. A. D. Amir, P. O. Krutzik, R. Finck, R. V. Bruggner, R. Melamed, A. Trejo, O. I. Ornatsky, R. S. Balderas, S. K. Plevritis, K. Sachs, D. Pe'er, S. D. Tanner, G. P. Nolan, Single-cell mass cytometry of differential immune and drug responses across a human hematopoietic continuum. *Science* **332**, 687–696 (2011).
36. R. Glaser, J. K. Kiecolt-Glaser, Stress-induced immune dysfunction: Implications for health. *Nat. Rev. Immunol.* **5**, 243–251 (2005).
37. N. Auphan, J. A. DiDonato, C. Rosette, A. Helmberg, M. Karin, Immunosuppression by glucocorticoids: Inhibition of NF-kappa B activity through induction of I kappa B synthesis. *Science* **270**, 286–290 (1995).
38. R. I. Scheinman, P. C. Cogswell, A. K. Lofquist, A. S. Baldwin Jr., Role of transcriptional activation of I kappa B alpha in mediation of immunosuppression by glucocorticoids. *Science* **270**, 283–286 (1995).
39. A. Biola, K. Andréau, M. David, M. Sturm, M. Haake, J. Bertoglio, M. Pallardy, The glucocorticoid receptor and STAT6 physically and functionally interact in T-lymphocytes. *FEBS Lett.* **487**, 229–233 (2000).
40. A. E. Coutinho, K. E. Chapman, The anti-inflammatory and immunosuppressive effects of glucocorticoids, recent developments and mechanistic insights. *Mol. Cell. Endocrinol.* **335**, 2–13 (2011).
41. M. Wang, M. N. Hill, L. Zhang, B. B. Gorzalka, C. J. Hillard, B. E. Alger, Acute restraint stress enhances hippocampal endocannabinoid function via glucocorticoid receptor activation. *J. Psychopharmacol.* **26**, 56–70 (2012).
42. C. J. Cook, Stress induces CRF release in the paraventricular nucleus, and both CRF and GABA release in the amygdala. *Physiol. Behav.* **82**, 751–762 (2004).
43. E. Elliott, G. Ezra-Nevo, L. Regev, A. Neufeld-Cohen, A. Chen, Resilience to social stress coincides with functional DNA methylation of the Crf gene in adult mice. *Nat. Neurosci.* **13**, 1351–1353 (2010).
44. S.-B. Li, N. Nevárez, W. J. Giardino, L. de Lecea, Optical probing of orexin/hypocretin receptor antagonists. *Sleep* **41**, (2018).
45. F. Naganuma, D. Kroeger, S. S. Bandaru, G. Absi, J. C. Madara, R. Vetrivelan, Lateral hypothalamic neurotensin neurons promote arousal and hyperthermia. *PLOS Biol.* **17**, e3000172 (2019).
46. T. L. Ben-Shaanan, H. Azulay-Debby, T. Dubovik, E. Starosvetsky, B. Korin, M. Schiller, N. L. Green, Y. Admon, F. Hakim, S. S. Shen-Orr, A. Rolls, Activation of the reward system boosts innate and adaptive immunity. *Nat. Med.* **22**, 940–944 (2016).
47. D. J. Taylor, K. L. Lichstein, H. H. Durrence, Insomnia as a health risk factor. *Behav. Sleep Med.* **1**, 227–247 (2003).
48. C. S. McAlpine, M. G. Kiss, S. Rattik, S. He, A. Vassalli, C. Valet, A. Anzai, C. T. Chan, J. E. Mindur, F. Kahles, W. C. Poller, V. Frodermann, A. M. Fenn, A. F. Gregory, L. Halle, Y. Iwamoto, F. F. Hoyer, C. J. Binder, P. Libby, M. Tafti, T. E. Scammell, M. Nahrendorf, F. K. Swirski, Sleep modulates haematopoiesis and protects against atherosclerosis. *Nature* **566**, 383–387 (2019).

49. L. A. Wang, D. H. Nguyen, S. W. Mifflin, Corticotropin-releasing hormone projections from the paraventricular nucleus of the hypothalamus to the nucleus of the solitary tract increase blood pressure. *J. Neurophysiol.* **121**, 602–608 (2019).
50. E. M. Friedman, M. R. Irwin, A role for CRH and the sympathetic nervous system in stress-induced immunosuppression. *Ann. N. Y. Acad. Sci.* **771**, 396–418 (1995).
51. M. L. Hanke, N. D. Powell, L. M. Stiner, M. T. Bailey, J. F. Sheridan, Beta adrenergic blockade decreases the immunomodulatory effects of social disruption stress. *Brain Behav. Immun.* **26**, 1150–1159 (2012).
52. X. Zhang, B. Lei, Y. Yuan, L. Zhang, L. Hu, S. Jin, B. Kang, X. Liao, W. Sun, F. Xu, Y. Zhong, J. Hu, H. Qi, Brain control of humoral immune responses amenable to behavioural modulation. *Nature* **581**, 204–208 (2020).
53. L. de Lecea, T. S. Kilduff, C. Peyron, X. B. Gao, P. E. Foye, P. E. Danielson, C. Fukuhara, E. L. F. Battenberg, V. T. Gautvik, F. S. Bartlett, W. N. Frankel, A. N. van den Pol, F. E. Bloom, K. M. Gautvik, J. G. Sutcliffe, The hypocretins: Hypothalamus-specific peptides with neuroexcitatory activity. *Proc. Natl. Acad. Sci. U.S.A.* **95**, 322–327 (1998).
54. T. Sakurai, A. Amemiya, M. Ishii, I. Matsuzaki, R. M. Chemelli, H. Tanaka, S. C. Williams, J. A. Richardson, G. P. Kozlowski, S. Wilson, J. R. S. Arch, R. E. Buckingham, A. C. Haynes, S. A. Carr, R. S. Annan, D. E. McNulty, W. S. Liu, J. A. Terrett, N. A. Elshourbagy, D. J. Bergsma, M. Yanagisawa, Orexins and orexin receptors: A family of hypothalamic neuropeptides and G protein-coupled receptors that regulate feeding behavior. *Cell* **92**, 573–585 (1998).
55. K. Labun, T. G. Montague, J. A. Gagnon, S. B. Thyme, E. Valen, CHOPCHOP v2: A web tool for the next generation of CRISPR genome engineering. *Nucleic Acids Res.* **44**, W272–W276 (2016).
56. F. A. Ran, P. D. Hsu, J. Wright, V. Agarwala, D. A. Scott, F. Zhang, Genome engineering using the CRISPR-Cas9 system. *Nat. Protoc.* **8**, 2281–2308 (2013).

Acknowledgments: We thank de Lecea laboratory members for the discussion, and A. Khan for excellent technical assistance. We also thank A. Olson and the Stanford Neuroscience Microscopy Service, NIH NS069375, for imaging technical support. **Funding:** This work was supported by NIH grants R01 MH102638 (L.d.L.), R01 MH116470 (L.d.L.), R01 HL150566 (L.d.L.), Stanford Alzheimer's Disease Center-Scully Family Seed Grant P50AG047366 (L.d.L.), and Stanford Department of Psychiatry and Behavioral Sciences Innovator Seed Grant (L.d.L.). J.C.B. was funded by NIMH F32 MH115431. B.G. was supported by the Stanford Department of Anesthesiology (FIDL grant). **Author contributions:** S.-B.L. and L.d.L. conceived and designed the research. S.-B.L., J.C.B., and H.Y. performed the experiments and analyzed the data. J.H. assisted in the CyTOF data analysis. B.G. supervised the CyTOF experiment and data analysis. L.d.L. supervised the entire project. S.-B.L. wrote the manuscript with contributions from J.C.B., B.G., and L.d.L. All authors discussed the results and commented on the manuscript. **Competing interests:** The authors declare that they have no competing interests. **Data and materials availability:** All data needed to evaluate the conclusions in the paper are present in the paper and/or the Supplementary Materials. The CyTOF datasets are publicly accessible at https://doi.org/10.5061/dryad.k3j9kd551. Additional data related to this paper may be requested with reasonable considerations.

Submitted 15 April 2020
Accepted 28 July 2020
Published 9 September 2020
10.1126/sciadv.abc2590

Citation: S.-B. Li, J. C. Borniger, H. Yamaguchi, J. Hédou, B. Gaudilliere, L. de Lecea, Hypothalamic circuitry underlying stress-induced insomnia and peripheral immunosuppression. *Sci. Adv.* **6**, eabc2590 (2020).